Chapter

# Electrical Endurance of Corona-Resistant Polyimide for Electrical Traction

*Tao Han and Andrea Cavallini*

## Abstract

This paper shows the behavior of several dielectric properties of corona-resistant polyimide tapes as a function of thermal (high temperatures) and ambient stress (high humidity coupled with high temperature). The main goal of the investigation is to understand and explain the evolution of the partial discharge endurance of the tapes as a function of nonelectrical aging. The results indicate that polyimide tapes are very stable up to temperatures of 320°C. However, the most elevated temperatures reduce the partial discharge endurance to 50% of the original value. This is probably due to morphological changes in the (outer) nanostructured layers of the tapes.

**Keywords:** electrical drives, insulation reliability, partial discharges, corona-resistant insulation, thermal aging

## 1. Introduction

Polyimide tapes are used to manufacture rotating machines. Due to their relatively large cost, these tapes are mostly in special machines exposed to high temperatures [1, 2]. As an example, machines used for drilling oil wells are insulated using PI enamels or tapes.

The situation is changing, however. Transport electrification is demanding more compact machines, characterized by higher power densities. This implies that electrical machines will be designed having higher frequencies, temperatures, and voltages compared with the current standards. This evolution places PI insulation in the forelight. As a matter of fact, aircraft turbine-mounted generators and train machines are already experiencing high temperatures, and many manufacturers already used PI-based commercial products (e.g., Kapton). Indeed, the use of PI wires has been challenged for aircraft wiring due to its sensitivity to hydrolysis, wet and dry arcing (it is speculated that PI exposed to arcing is prone to catch fire prior than reaching a failure [3, 4]).

PI tapes can be used as slot liners (generally in form of laminates as NKN), phase separators, as well us around conductors to realize the phase-to-ground, phase-to-phase, and turn-to-turn insulation. In the last case, adhesive tapes are usually wrapped around the conductor. Complete adhesion is achieved by microwave heating of the conductor first and then infrared heating of the outer part. Eventually, the conductor is cooled down rapidly by immersion.

To date, most electrical machines are inserted in power electronic drives and are fed by a power electronic converter (inverter). The waveform provided by inverters is not the standard sinusoidal waveform, but a train of voltage impulses whose fundamental frequency is equal to the frequency of the reference sinusoidal voltage waveform. This type of voltage is sketched in **Figure 1**.

The advantages of PWM inverters are so many that nowadays only very few motors are still connected to the AC grid directly. As an example, the frequency of the drive is regulated in a straightforward way by changing the frequency of the reference voltage waveform. Furthermore, the maximum frequency of the drive can be much higher than that of the power grid, being the latter selected based on the limits of large rotating machines and with transmission losses and limits as a target. Going to higher frequencies ensures the possibility of shrinking the magnetic circuit of the motor, reducing the weight and the volume of the machine. Both advantages (controllability, high power densities) are vital for transport electrification to ensure that the drive works smoothly using a light actuator.

The "dark side" of PWM waveforms, however, is the electrical stress they impose on the insulation [5–8]. The voltage at the motor terminals can increase due to wave reflections when the voltage impulses reach the machine. This is because the connecting cables have a characteristic impedance of 20–30 Ω, whereas the machine characteristic impedance can be up to 400 Ω. Furthermore, a phenomenon known as "double pulse," which happens when two phases commutate simultaneously, can further raise the applied voltage. The theoretical limits of these phenomena are (a) the voltage can be doubled when only reflections occur and (b) the voltage can be four times larger if both reflection and double pulse occur (**Figure 2**).

Furthermore, the impulses must propagate within the winding of the machine, which are complex inductive capacitive networks. Without going into details, it is important to understand that, during the rising and falling flanks of the voltage impulses, the first coil of the machine will withstand most of the inverter voltage, whereas if Nc is the number of coils in the machine, all coils will be subjected to the same voltage V/Nc when subjected to AC voltage waveforms.

This change in the electrical stress levels brought about a radical change in the failure mode of low-voltage rotating machines. Prior to the advent of power electronics, insulation mostly failed due to thermal aging. The eventual failure mode was the opening of crack where a large leakage current, able to melt the dielectric,

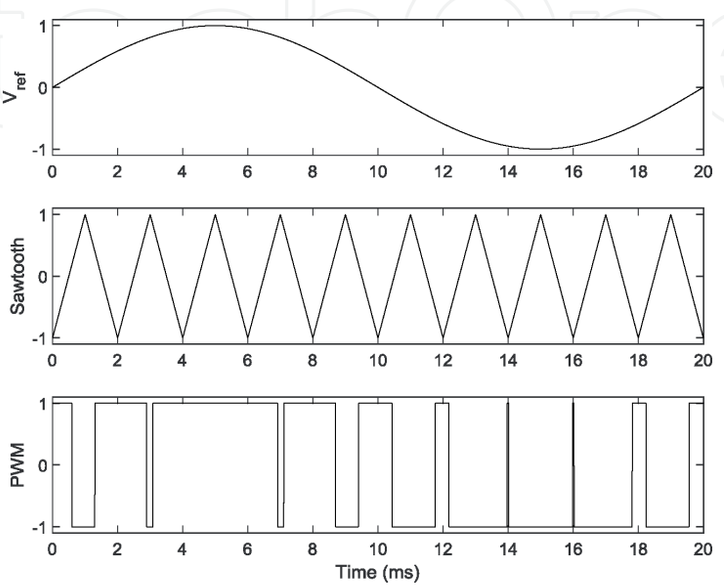


**Figure 1.**
*PWM voltage waveform.*

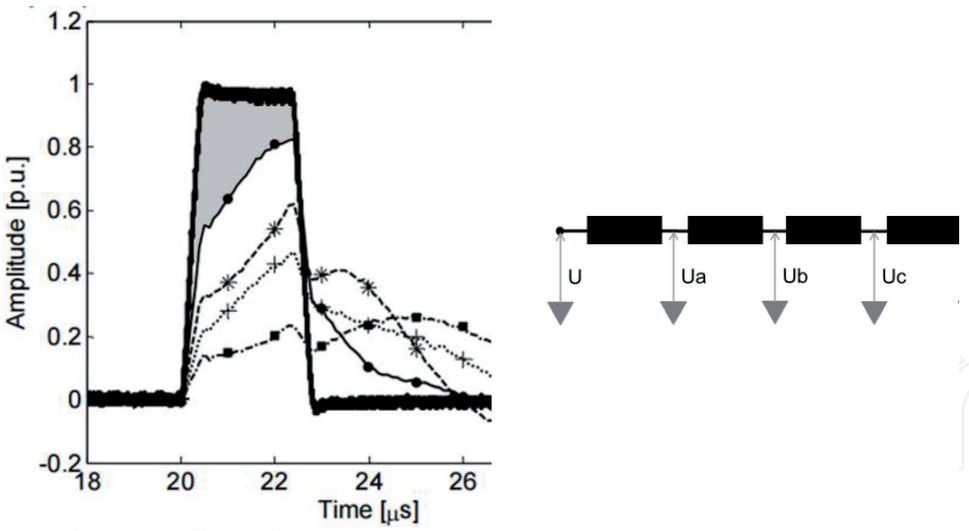


**Figure 2.**
*Potential at a five-coil low-voltage motor terminal (U) and at the interconnection between adjacent coils (Ua, Ub, Uc, Ud). In gray, the voltage drops across the first coil.*

could flow. Under power electronics, if the electrical stress exceeds a critical threshold, partial discharges are incepted inside the winding. These discharges can occur with a very large repetition frequency, comparable with the switching frequency of the power converter.

The insulation that is most vulnerable to partial discharges is the turn insulation [9, 10], as often enamels or tapes having limited thickness are used (thus, it is easier to puncture the insulation, and, moreover, the electric fields are the highest in the machine when inverters are used). Dielectrics made of purely organic polymers degrade quickly under PD bombardment as the C–C and C–H bond energies are 3–4 eV, and a large percentage of electrons in the discharge have sufficient energy to cause dissociative electron attachment (DEA) leading to bond breaking and free radical formation [11, 12]. After long enough, this process leads to the puncture of the insulation.

Due to these considerations, dielectrics used for the turn insulation of rotating machines have been nanostructured, meaning that inorganic particles of nanometric size were added to the base polymer [13, 14]. Nanostructured insulation for rotating machines is often indicated as corona-resistant insulation (e.g., CR wires, CR tapes, CR laminates, etc.).These particles tend to form a barrier to the progressive degradation induced by partial discharge activity (as an example, the formation of ceramic-like layers has been observed on the outer surface of CR winding wires). CR PI tapes have been proposed as a solution to improve the reliability of inverter-fed machines [15, 16]. Besides these tapes can be of use also in medium-voltage machines, where the large fields in the phase-to-ground insulation can lead to partial discharges in proximity of the conductors if the insulation detaches from the conductor due to the combined effect of high temperatures and thermal cycling (in that case, an air pocket can form in proximity of the conductor, leading to the inception of partial discharges that, in the long term, can cause a failure of the turn insulation).

The superior performance of CR insulation compared to standard insulation has been proven in literature [13, 16]. However, all the tests were conducted on pristine CR insulation. As this book is being written, activities are under way to test CR winding wires using repetitive voltage impulses and temperatures of 155°C. The limit of this approach is that CR insulation systems are compared in the absence of thermal aging. As a matter of fact, the partial discharge endurance tests are

relatively short, and the oven temperature is well below the class temperature (that can be 180°C, 200°C, 220°C, or 240°C). This implies that the dielectric will not undergo a significant amount of oxidation or other forms of chemical degradation. Besides, the impact of hydrolysis will not be accounted for. As a result, it will not be easy to extrapolate the results to practical applications, as the combined electrical-thermal-ambient stress will differ substantially from the tests experienced during the tests.

In order to show how these stresses can alter the endurance of PI insulation to PD activity, we shall discuss in the forthcoming sections experiments carried out on CR Kapton films subjected to thermal and ambient stress and tested at regular times for PD endurance. The results will highlight the most likely phenomenon leading to a significant reduction of the endurance properties.

## 2. Test structure

### 2.1 Test sequence

The tests were programmed in sequences, to show the progressive deterioration (if any) of the PI properties. The test logic is shown in **Figure 3** and follows the ideas reported in [17]. Aging is subdivided in aging sub-cycles followed by diagnostic sub-cycles. During the diagnostic sub-cycles, measurements apt to infer the degradation of the PI films as electrical insulators are carried out. The samples that during the tests are modified by the test itself are discarded, and aging continues with the remaining samples. Therefore, PI films were prepared in large numbers to ensure that aging tests could be performed on different samples to highlight the degradation of PI dielectric properties (and not the effect of previous tests).

### 2.2 Measurements

The tests were performed on corona-resistant PI tapes (Dupont Kapton 200 CR), having nominal thickness of 50 μm. During the diagnostic sub-cycles, the following quantities were measured/reported (**Figure 4**):

1. Visual appearance of the sample.

2. Thickness evaluated by means of a micrometric screw.

3. Dielectric spectroscopy in the range of 0.1–3 MHz. The specimens were extracted from the aging cell and covered with silver paint. Since elevated temperatures could affect the silver paint, samples were discarded after testing.

4. Bulk DC conductivity using a three-electrode system. The electric field was 15 kV/mm.

5. PDIV measurements were carried out using a 50 Hz sinusoidal supply voltage. A rod/plane electrode configuration was designed and manufactured following [18]. The PD sensor was a high-frequency current transformer (HFCT). A Techimp PDBase II detector (bandwidth 50 MHz, sampling rate 200 MSa/s, and vertical resolution 12 bit) was employed to detect PD. The sensitivity was better than 5 pC. During the PDIV tests, the samples were held in a climatic chamber at 20°C, 25% relative humidity. The voltage was increased in steps of

50 V each lasting 30 s. PDIV measurements were repeated eight times, each time changing the position of the rod electrode. The PDIV measurement setup is outlined in **Figure 1**. Samples were discarded after testing.

6. Partial discharge endurance tests were carried out on all the samples. The supply voltage was a 1 kHz unipolar square wave. The peak-to-peak voltage was 7 kV. The rod/plane electrode configuration is the same used in the PDIV tests. Samples were discarded after the tests [18].

### 2.3 Aging stresses, levels, and timings

A first round of tests was performed placing the sample in the oven at a temperature of 270°C for 864 h. Indeed, as it will be exposed in the next section, 270°C is too a low temperature to produce a remarkable aging in PI samples (**Table 1**). Therefore, a second aging cycle lasting 294 h was performed. Knowing the potential negative impact of hydrolysis on PI films, this cycle was carried out placing the samples in a climatic chamber at 80°C with a relative humidity of 80%. Eventually, a last cycle lasting 432 h was carried out placing the samples in the oven at 320°C.

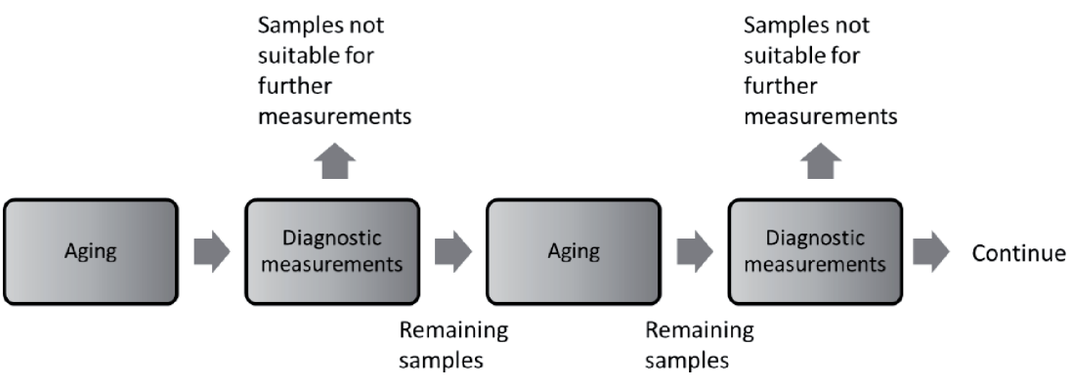


**Figure 3.**
*Test plan for thermal aging at 270°C.*

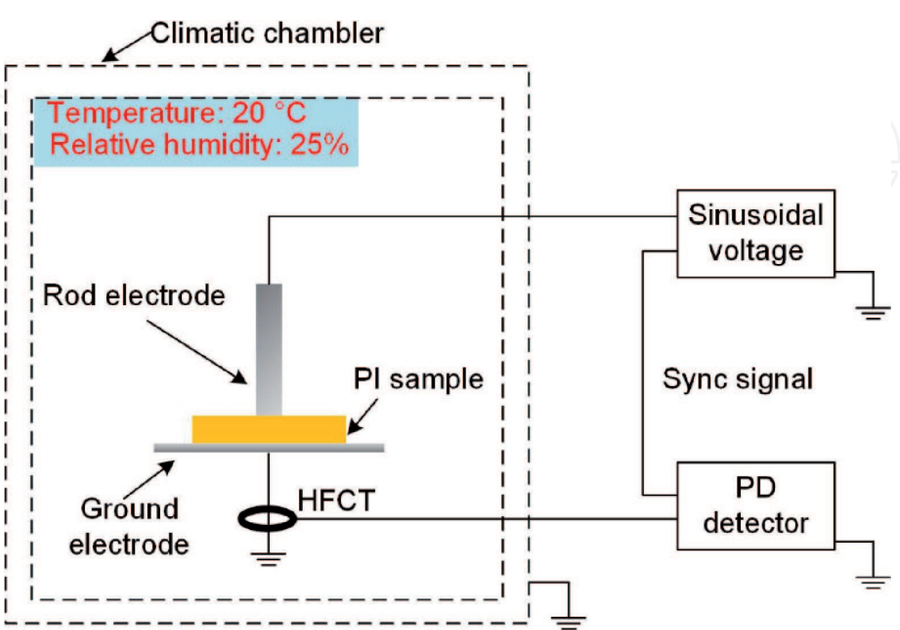


**Figure 4.**
*Test cell for PDIV tests.*

| Aging stage | Time (h) | Condition |
|---|---|---|
| 1 | 864 | 270°C |
| 2 | 294 | 80°C and 80% RH |
| 3 | 432 | 320°C |

**Table 1.**
*Thermal aging processes.*

## 3. Results

### 3.1 Dielectric spectroscopy

To check the dielectric characteristics during each aging stage, the dielectric spectroscopy test was employed. **Figures 5** and **6** show the real and imaginary parts of the permittivity (ε' and ε"). It can be found that both ε' and ε" change to some extent in stage 1. More notable increases can be found in aging stage 2, particularly for frequencies below 100 Hz. ε' reaches a value of ~7.0 at low frequency. During aging stage 2, the outer layer (nanocomposites) was exposed in high temperature and humidity, where hydrolysis and water absorption will occur as a result [19, 20]. The polar production after hydrolysis and absorbed water (with ε' of ~80) contributes to the increased ε' and ε". After, in stage 3, the sample was kept in oven at 320°C. The acid and amine groups formed by hydrolysis can be recombined, and the absorbed water will be removed in a short time [21]. As a result, the dielectric response was reverted to be near to that of PI without aging.

To get more details of the changing dielectric properties, ε' and ε" of some selected frequencies are shown in **Figures 7** and **8**. As shown in **Figure 7**, the increasing ε' can be found in the first 576 h in stage 1, while it decreases till the end of this stage. A peak value of ε' at each frequency can be confirmed in stage 2, which indicates that the aging parameters of stage 2 affect the dielectric properties

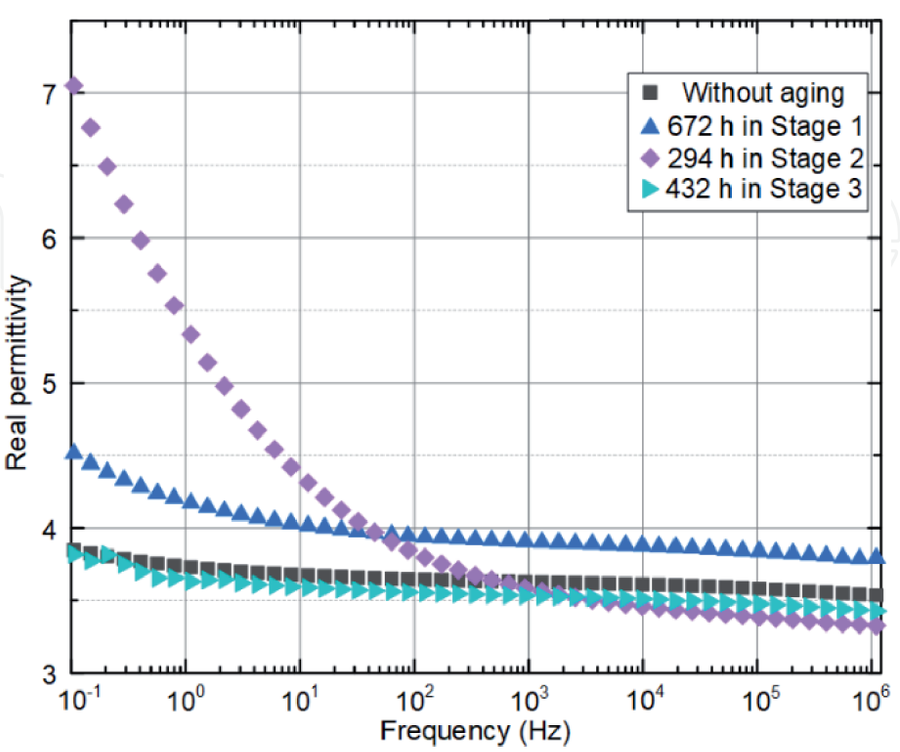


**Figure 5.**
*Real permittivity at the end of each aging stage.*

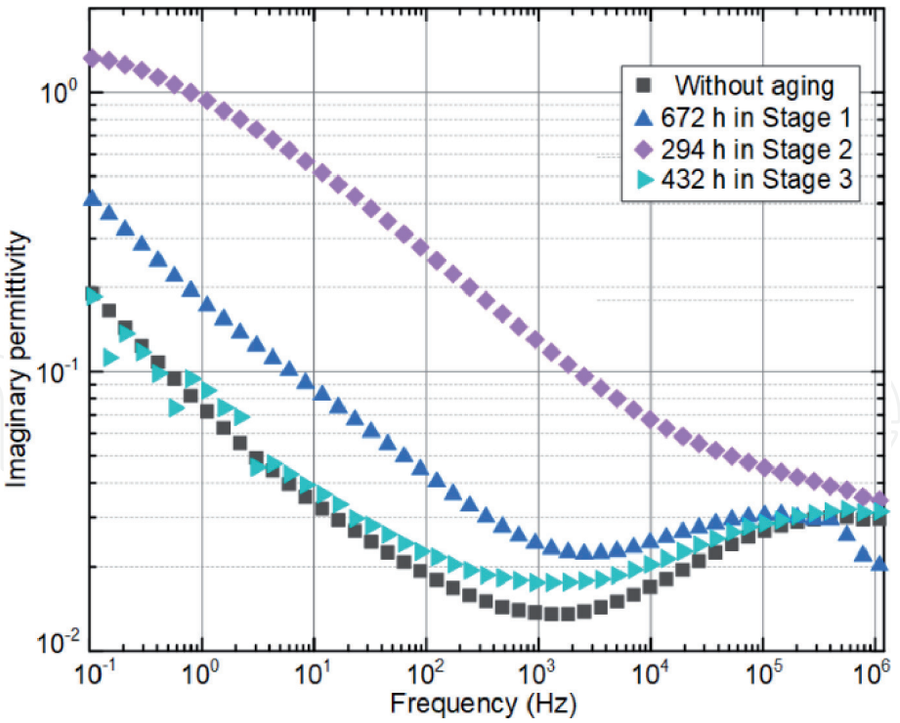


**Figure 6.**
*Imaginary permittivity at the end of each aging stage.*

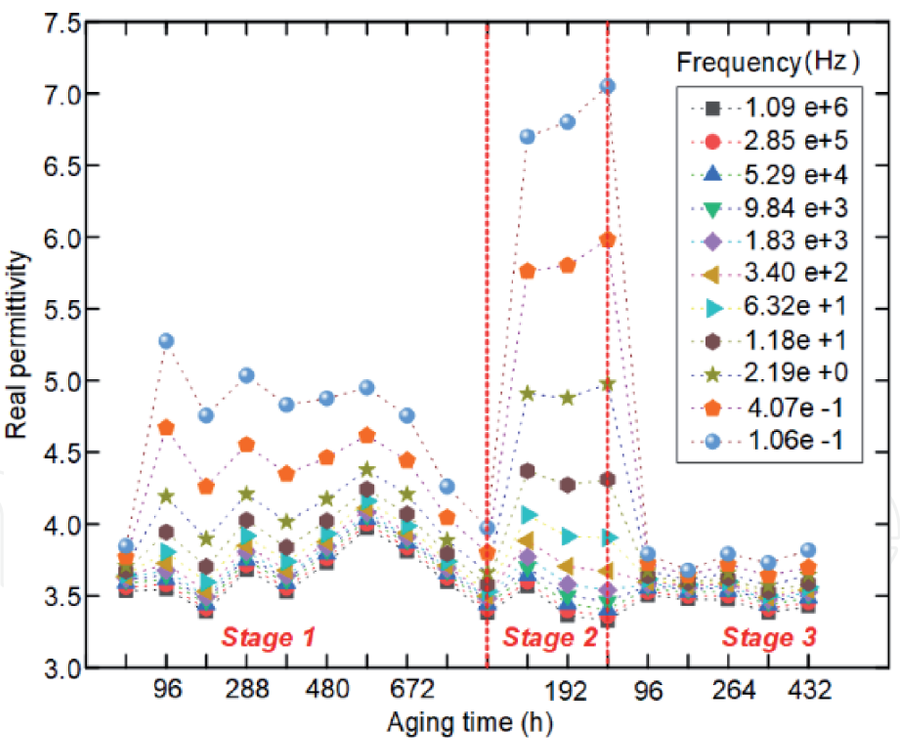


**Figure 7.**
*Trend of ε' at different frequencies and different aging stages.*

obviously. In contrast, ε' at each stage is stable in the whole stage 3. As shown in **Figure 8**, a similar tendency can be found in ε".

### 3.2 Bulk conductivity

Bulk conductivity of PI in the three aging stages is reported in **Figure 9**. Before aging, PI samples have a conductivity below $10^{-15}$ S/m. During stage 1

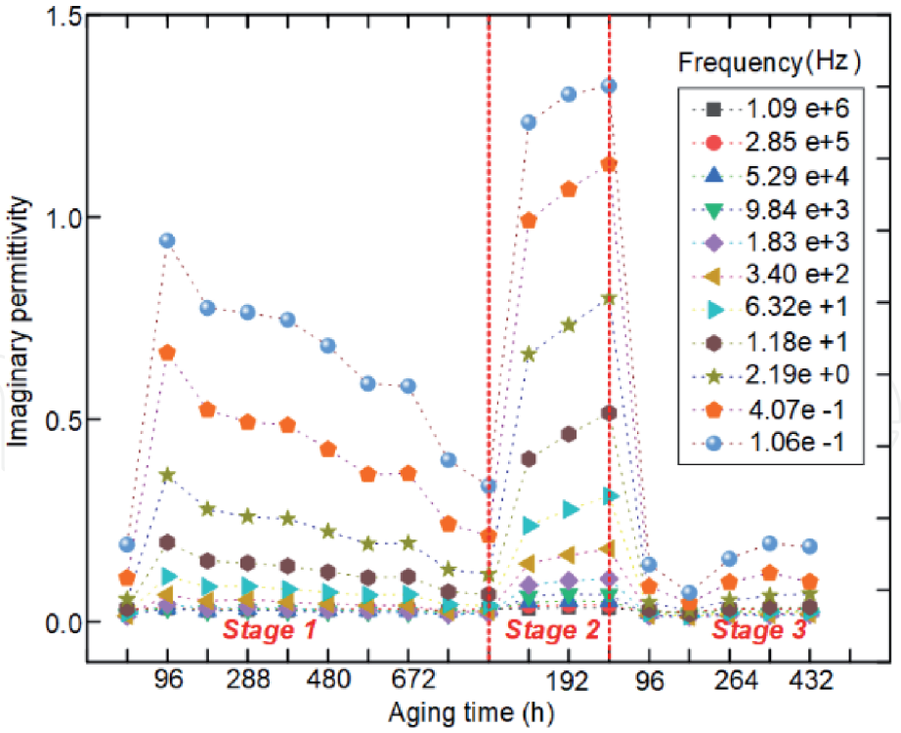


**Figure 8.**
*Trend of ε" at different frequencies and different aging stages.*

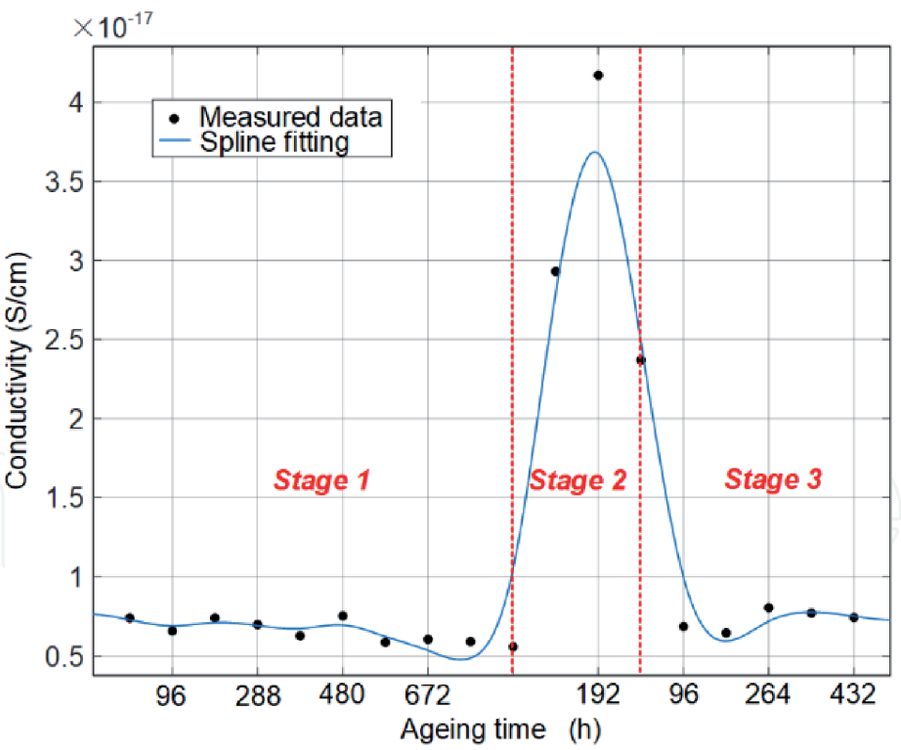


**Figure 9.**
*Change of bulk conductivity with aging stage.*

(thermal aging at 270°C) there might be a decrease of conductivity (~25%). After hydrolysis and moisture absorption (stage 2, T = 80°C, RH = 80%), the conductivity increases by an order of magnitude. In stage 3 (thermal aging at 320°C), the moisture is removed, and the chemical structure is restored [21]. The conductivity returns to the initial value, a finding in agreement with the results reported in [19].

In summary, the conductivity of PI is stable with thermal aging up to 320°C. However, high humidity levels in the operating environment might cause an increase of conductivity, particularly if the machine has not been used for some time.

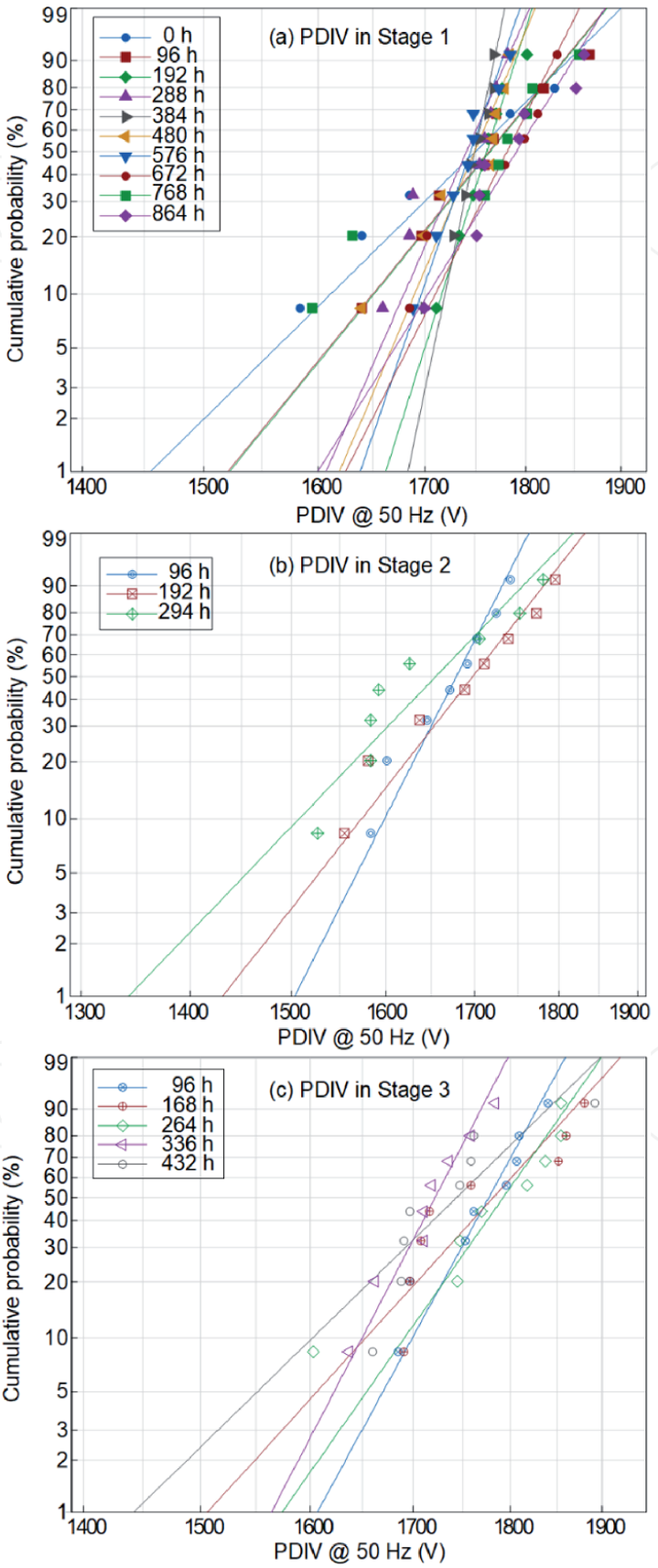


**Figure 10.**
*Weibull plots of PDIV results in all aging stages.*

### 3.3 PDIV results

PDIV tests were carried out with AC of 50 Hz. Eight specimens were tested at each aging time. The peak-to-peak value of applied voltage is recorded for the PDIV. All the data of each aging time are Weibull plotted and shown in **Figure 10**. The B10 parameter is employed here, which means the 10% probability of PD occurrence. Besides, the Weibull scale parameter (α) and shape parameter (β) are also employed and shown in **Table 2**.

From the estimation of Weibull plot, B10 and α can be calculated at each aging time. In stage 1 shown in **Figure 10(a)**, B10 changes from 1590 (at 0 h) to 1715 V (at 192 h), while α varies from 1750 to 1810 V. It indicates that B10 is more scattered after the thermal aging at 270°C. In stage 2 shown in **Figure 10(b)**, both B10 and α show similar behavior, while in stage 3 (**Figure 10(c)**), both B10 and α are scattered, compared with the other two stages.

B10 can be employed to show the reliability of PI in severe working conditions. As shown in **Figure 11**, this "reliability" can be divided into three stages corresponding to the three aging stages. B10 increases sharply in the first 200 h, and then it becomes stable till the end of stage 1. With the beginning of stage 2, the high humidity makes B10 drop linearly with aging time, which indicates the risk of PI application in wet environment. As mentioned above, the high temperature in stage 3 will recombine the PI chains and remove the moisture in the bulk, resulting in the recovery of B10. However, a decrease of B10 occurs after its recovery, from 1680 to 1640 V.

| Aging stage | Time under stress (h) | B10 (Vpp) | α (Vpp) | β |
|---|---|---|---|---|
| (I) T = 270°C | 0 | 1590 | 1780 | 19.9 |
| | 96 | 1646 | 1786 | 27.6 |
| | 192 | 1715 | 1770 | 70.8 |
| | 288 | 1663 | 1754 | 42.4 |
| | 384 | 1710 | 1756 | 83.6 |
| | 480 | 1664 | 1764 | 38.8 |
| | 576 | 1692 | 1755 | 61.5 |
| | 672 | 1689 | 1797 | 36.3 |
| | 768 | 1615 | 1790 | 21.9 |
| | 864 | 1702 | 1808 | 37.5 |
| (II) T = 80°C, RH = 80% | 96 | 1583 | 1696 | 32.5 |
| | 192 | 1551 | 1725 | 21.2 |
| | 294 | 1514 | 1682 | 21.3 |
| (III) T = 320°C | 96 | 1684 | 1794 | 35.6 |
| | 168 | 1660 | 1803 | 27.2 |
| | 264 | 1652 | 1817 | 23.6 |
| | 336 | 1642 | 1737 | 39.8 |
| | 432 | 1641 | 1766 | 30.7 |

**Table 2.**
*PDIV statistics during aging (N = 8).*

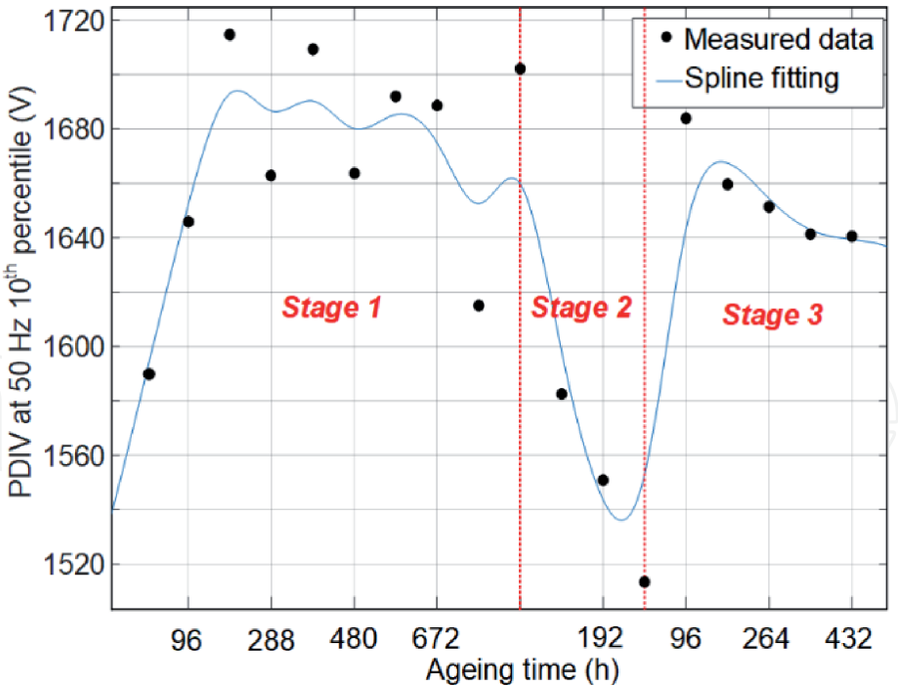


**Figure 11.**
*Trend of PDIV B10 of at 50 Hz during aging.*

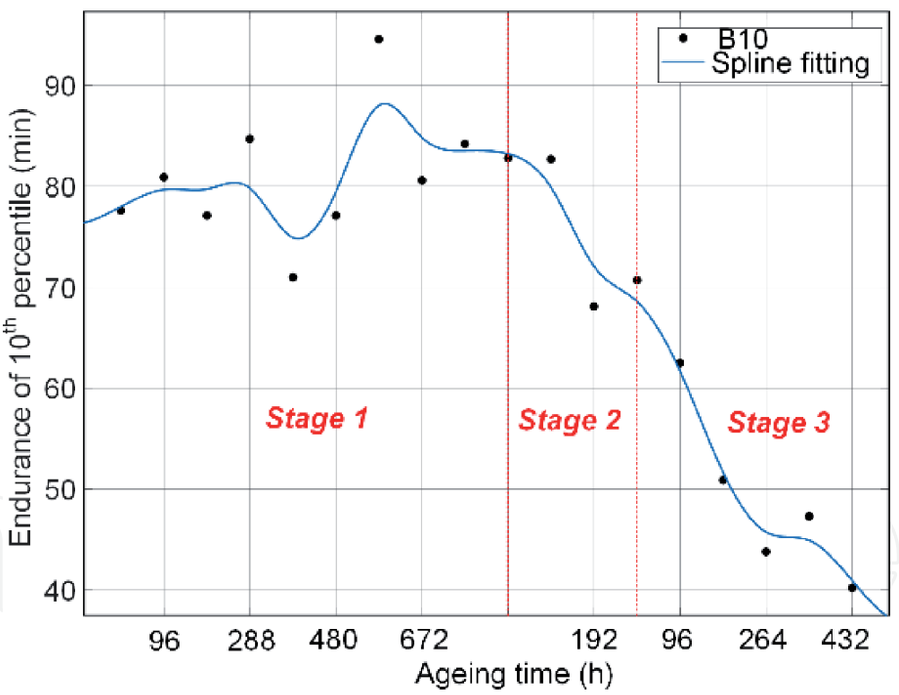


**Figure 12.**
*B10 of PD endurance in all the stages.*

By checking **Figures 5, 7** and **11**, one can find that B10 is closely related to the change of ε'. A capacitor model can be used here to explain this relation. In this model, the air gap between rod electrode and sample surface is equivalent to a capacitor, the PI tape to another one. With the increasing ε' of PI, the electric field in air gap will increase simultaneously. For instance, the ε' at 50 Hz increases 8% (from ~3.8 to ~4.0) in stage 2; B10 in **Figure 11** decreases from 1660 to 1520 V (~9%) correspondingly.

### 3.4 PD endurance under impulse voltages

PD endurance time tests were carried out under a square wave with a peak-to-peak voltage of 7 kV. After the application of this voltage, a corona will be found around the rod electrode, destroying the PI tape and leading to breakdown. This voltage parameter was selected for the purpose of achieving breakdown within less than 2 h.

Eight samples were tested at each aging time. The Weibull plots were employed, and B10 of endurance time was calculated. B10 of all the stages are shown in **Figure 12**. B10 in stage 1 varies from 70 to 95 min; this fluctuation is maybe caused by the limitation of sample quantity. In stage 2, the trend is obvious. B10 decreases from 83 to 68 min. While in stage 3, B10 declines linearly with aging time, from 68 to 40 min. It can be found that thermal aging in stage 1 will not change the endurance of PI. The reason of decreasing endurance in stage 2 is assumed to be the reduction of PDIV. However, endurance in stage 3 also decreases, while the PDIV is recovered to the initial level. This change is more likely related to the material changes inside the sample caused by thermal aging, which will be discussed in the next section.

## 4. Discussion

The excellent results achieved by Kapton 200 CR exposed to high temperature could have been, somehow, predicted by a thermogravimetric analysis (TGA). The weight loss of Kapton tapes is negligible below 500°C, as shown in **Figure 13**, confirming the high thermal stability of the tapes.

The Fourier transform infrared (FTIR) spectroscopy of pristine and aged samples is reported in **Figure 14**. Without knowing exactly the chemical structure of the tapes, it is difficult to trace back the FTIR peaks to the corresponding chemical species. Yet, the peak sequence does not appear to be modified in an appreciable way through the series of aging cycles, suggesting that the chemical structure is stable. This is another confirmation that the Kapton 200 CR tapes did not change in a remarkable way their structure during the aging.

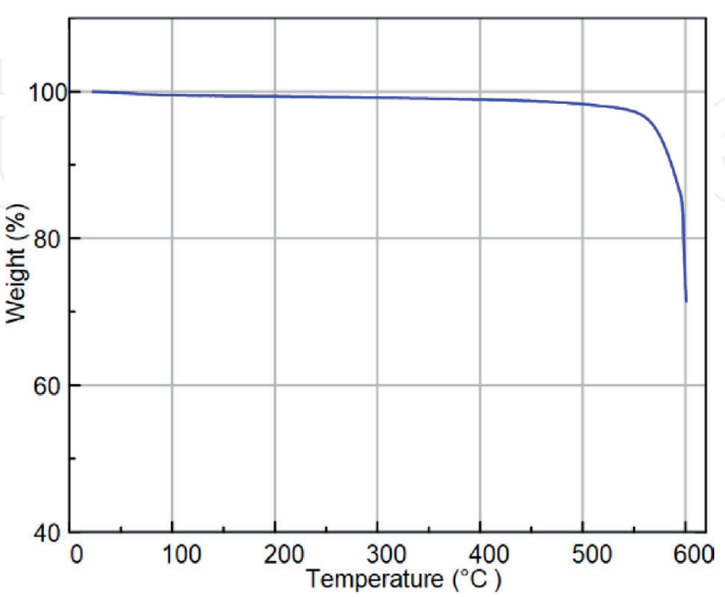


**Figure 13.**
*TGA test of PI samples.*

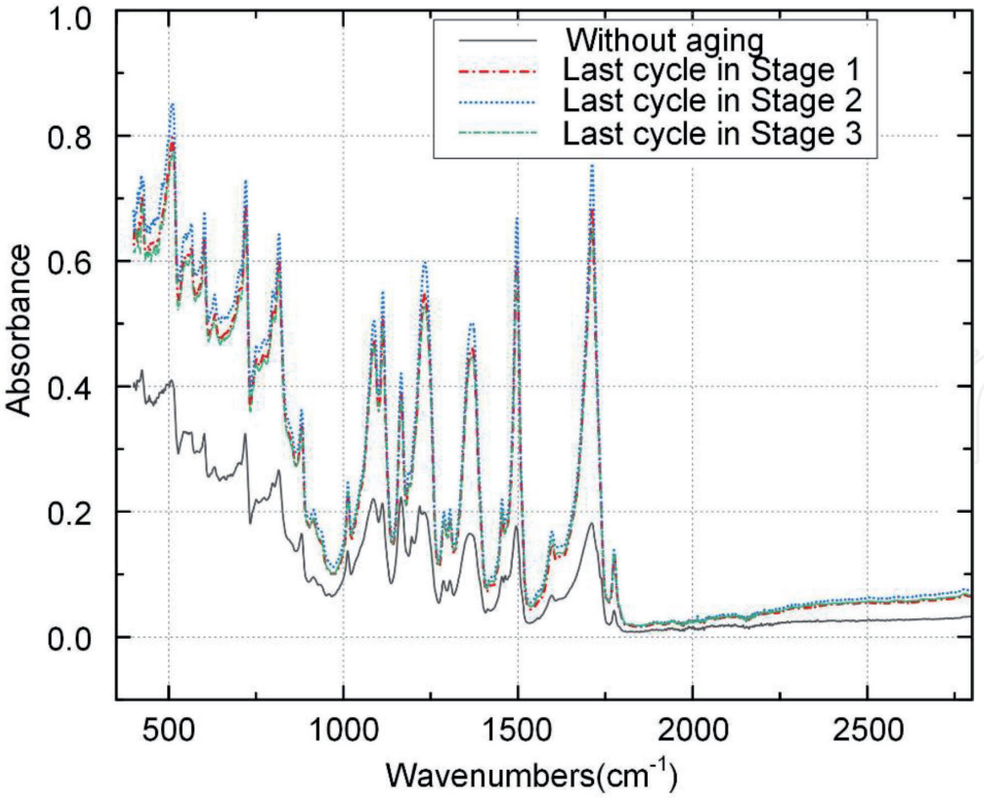


**Figure 14.**
*FTIR spectroscopy of pristine and aged Kapton samples.*

Both TGA and FTIR suggest that little changed in the PI tapes during changes. Yet, partial discharge endurance halved, with a sharp reduction in stage 3 (300°C). As the chemistry of the material seems to play a marginal role in this phenomenon, it was decided to inspect the morphology of the samples. In a nanostructured dielectric, inorganic nanoparticles are bonded to the polymeric matrix through a coupling agent able to confer a good stability to the resulting structure. Above a critical temperature, the bonds between the host matrix and the nanoparticles can break, enabling the nanoparticles to rearrange. The scanning electron microscope (SEM) imaging was thus used to investigate whether this kind of phenomena was taking place in the sample tapes. To do that, SEM pictures of the surface and of the cross section of both pristine and aged tapes were taken. The pictures of the cross section were obtained by immersing the tapes in liquid nitrogen and then cracking them.

The SEM pictures of pristine and aged sample surfaces at two magnification levels (5000× and 50,000×) are shown in **Figure 15**. The 5000× image does not reveal any specific sign of aging. The 50,000× picture highlights the presence of nanoparticles (white spots) in contrast with the host matrix. No appreciable sign of deterioration can be observed.

**Figure 16** shows the cross section of the samples. At the lowest magnification level (5000×), it can be appreciated that the tapes are probably a three-layer structure. It can be guessed that the central layer is pure PI, conferring elasticity to the tapes (in general, nanostructured materials tend to be less elastic than the host matrix). The outer layer consists of nanostructured PI, to ensure electrical endurance.

At the lowest magnification level (50,000×), signs of reorganization of the nanostructured layers can be observed. Apparently, the nanoparticles appear more

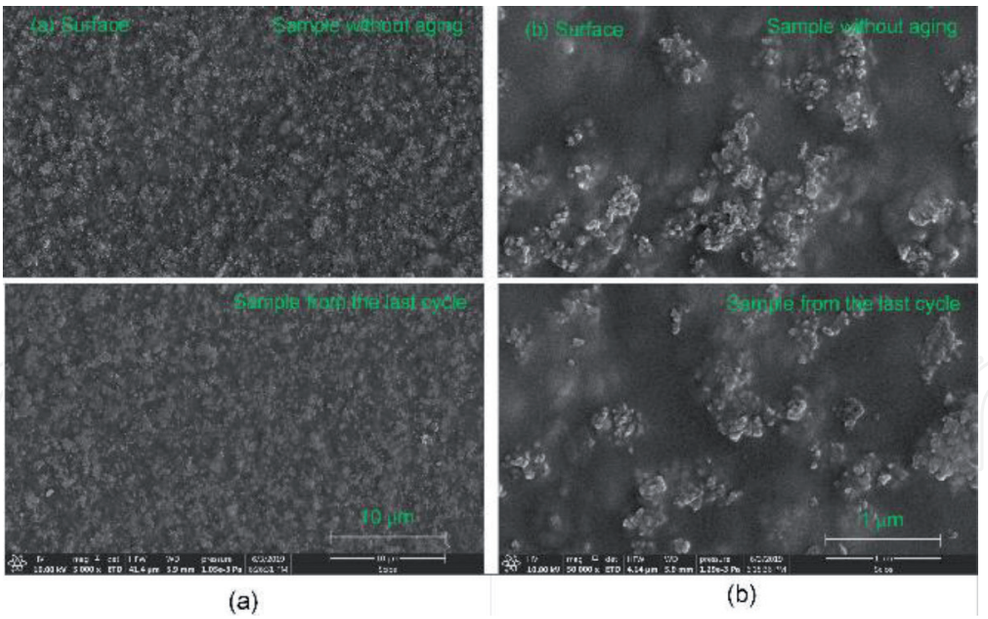


**Figure 15.**
*SEM images of the surface of samples virgin and at the end of aging stage 3. (a) and (b) are pictures obtained with magnification of 5000× and 50,000×, respectively.*

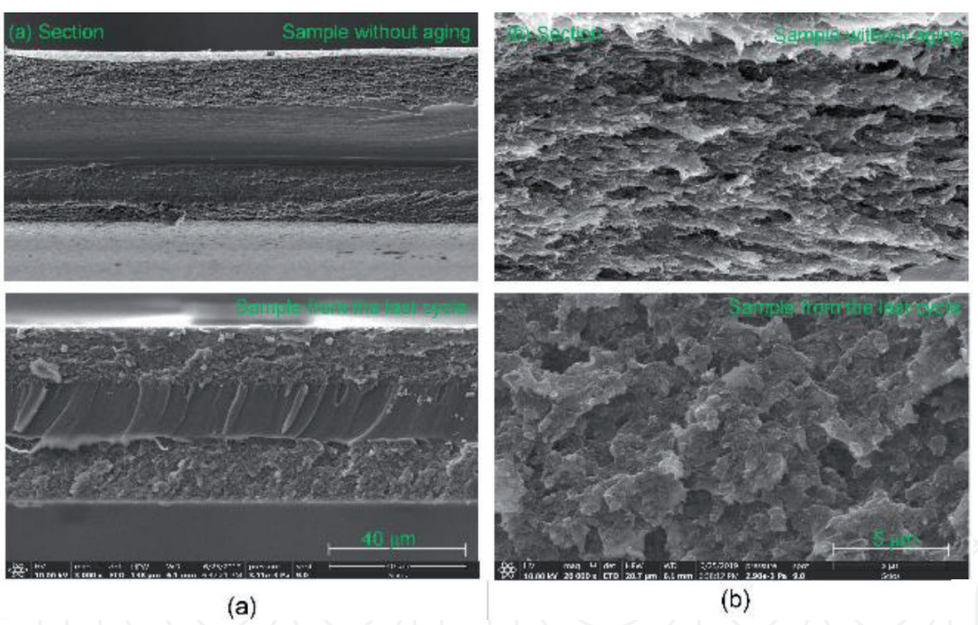


**Figure 16.**
*SEM images of the crack surface of samples virgin and at the end of aging stage 3. (a) and (b) are pictures obtained with magnification of 5000× and 50,000×, respectively.*

randomly oriented and with the tendency to form agglomerations. Therefore, regions where the host matrix becomes predominant are created. In these regions, partial discharge erosion can take place more easily leading to a reduction of the partial discharge endurance of the tapes.

These morphological changes could be addressed to the temperatures above 300°C which might have caused the stripping of the nanoparticle/host matrix bonding agent. Besides, the outer layer might have a differential thermal expansion coefficient compared with the central layer. At a microscopical level, the different expansions of the layers might have helped the distortion of the structure (the orientation of the clusters in the picture at 5000× seems to change from horizontal to skewed after aging).

## 5. Conclusions

Polyimide tapes have excellent properties that make them ideal choice to manufacture the turn insulation of form wound machines (both low-voltage hairpin machines used, e.g., in traction electrification and medium-voltage machines). Indeed, the final insulation class of the insulation system could be lower than that of the polyimide tapes, as it will be difficult (or extremely costly) to find a whole set of materials (enamels, slot liners, phase separators, wedges, sleeving, varnish or resin, conductive armor tape, stress control tapes) able to achieve the same thermal performance of the turn insulating. The results reported here confirm the capability of PI tapes to withstand extreme temperatures for long times. Exposing PI to temperatures above 300°C, moreover, has a positive effect as the acid and amine groups formed by hydrolysis reconnect, restoring the polymeric chains. Indeed, hydrolyzed PI displays a higher relative permittivity than the pristine tapes (4 versus 3.5 at 50 Hz), leading to a reduction of the partial discharge inception voltage (90%). A possible negative effect observed after thermal aging at 270°C is a general increase of the relative permittivity that would also lead to a reduction of PDIV, although more moderate than that induced by hydrolysis.

The electrical endurance tests highlight the excellent capability of PI corona-resistant (CR) materials to withstand partial discharge bombardment. The apparent short times (from 80 min at the beginning of the test to 40 min after the three stages of aging) should be weighed against the large electrical stress used for the tests (7 kV/100 μm = 140 kV/mm within the PI), a stress level hardly experienced in electrical machinery. Thermal aging seems to have a limited impact on the electrical endurance unless the PI is exposed to temperatures above 300°C for long times. By inspecting pristine and aged tapes using the scanning electron microscope, the electrical endurance of the CR PI tapes was explained by a three-layer structure of the tapes: a central layer of PI serves the purpose of conferring flexibility to the tapes, and two nanostructured outer layers ensure resistance to partial discharge bombardment. Aging at 300°C seems to have an impact on the morphology of the nanostructured layers, leading to a substantial (50%) reduction of the electrical endurance of the tapes.

## Author details

Tao Han[1] and Andrea Cavallini[2]*

1 School of Electrical and Information Engineering, Tianjin University, Tianjin, China

2 University of Bologna, Bologna, Italy

*Address all correspondence to: andrea.cavallini@unibo.it

## References

[1] Liaw DJ, Wang KL, Huang YC, Lee KR, Lai JY, Ha CS. Advanced polyimide materials: syntheses, physical properties and applications. Progress in Polymer Science. 2012;**37**(7):907-974. DOI: 10.1016/j.progpolymsci.2012.02.005

[2] Abadie MJM. High Performance Polymers–Polyimides Based–From Chemistry to Applications. Riheca, CA: IntechOpen; 2012

[3] Piloian M. What are the disadvantages of Kapton insulated wire?. Available from: https://www.interconnect-wiring.com/blog/disadvantages-kapton-insulated-wire/

[4] Paterson A. Kapton A Dangerous Aircraft Wiring Product implicated in aircraft electrical fires. Available from: http://vision.net.au/~apaterson/aviation/kapton_mangold.htm

[5] Persson E. Transient effects in the application of PWM inverters to induction motors. IEEE Transactions on Industry Applications. 1992;**28**:1095-1101

[6] Oliver JA, Stone GC. Implications for the application of adjustable speed drive electronics to the motor stator winding insulation. IEEE Electrical Insulation Magazine. 1995;**11**(4):32-36

[7] Stone GC, Campbell S, Tetreault S. Inverter-fed drives: Which motor stators are at risk? IEEE Industry Applications Magazine. 2000;**6**:17-22

[8] Wheeler JCG. Effects of converter pulses on the electrical insulation in low and medium voltage motors. IEEE Electrical Insulation Magazine. 2005;**21**(2):22-29

[9] Kaufhold M, Borner G, Eberhardt M, Speck J. Failure mechanism of the inter-turn insulation of low voltage electric machines fed by pulse-controlled inverters. IEEE Electrical Insulation Magazine. 1996;**12**(5):9-16

[10] Yin W. Failure mechanism of winding insulation in inverter-fed motors. IEEE Electrical Insulation Magazine. 1997;**13**(6):18-23

[11] Sanche L. Nanoscopic aspects of electronic aging in dielectrics. IEEE Transactions on Dielectrics and Electrical Insulation. 1997;**4**(5):507-543

[12] Serra S, Montanari GC, Mazzanti G. Theory of inception mechanism and growth of defect-induced damage in polyethylene cable insulation. Journal of Applied Physics. 2005;**98**(3):034102

[13] Hayakawa N, Okubo H. Lifetime characteristics of nanocomposite enameled wire under surge voltage application [feature article]. IEEE Electrical Insulation Magazine. 2008;**24**(2):22-27

[14] Fabiani D. Accelerated degradation of AC motor insulation due to voltage waveforms generated by adjustable speed drives. [Ph.D. Thesis], 2002, Gedit Edizioni, Bologna, May 2003

[15] Corona Resistant Kapton CR Takes Electrical Insulation Design and Reliability to New Levels [Online]. Available from: https://www.dupont.com/products/kapton-cr.html

[16] Wu GN, Wu J, Zhou L, Gao B, Zhou K, Guo X, et al. Microscopic view of aging mechanism of polyimide film under pulse voltage in presence of partial discharge. IEEE Transactions on Dielectrics and Electrical Insulation. 2010;**17**(1):125-132. DOI: 10.1109/TDEI.2010.5412010

[17] Rotating Electrical Machines—Part 18-41: Partial Discharge Free Electrical Insulation Systems (Type I) Used in

Rotating Electrical Machines Fed from Voltage Converters—Qualification and Quality Control Tests. IEC TS. 2007;60034:18-41

[18] IEC 60343. Recommended Test Methods for Determining the Relative Resistance of Insulating Materials to Breakdown by Surface Discharges. 1991

[19] Khazaka R, Locatelli ML, Diaham S, Bidan P. Endurance of thin insulation polyimide films for high-temperature power module applications. IEEE Transactions on Components, Packaging and Manufacturing Technology. 2013;**3**(5):811-817

[20] Li L, Bowler N, Hondred PR, Kessler MR. Statistical analysis of electrical breakdown behavior of polyimide following degrading processes. IEEE Transactions on Dielectrics and Electrical Insulation. 2011;**18**(6):1955-1962

[21] Punderson JO, Heacock JF. Polyimide film insulation for aerospace wire and cable: Why long-term performance exceeds some limited laboratory projections. In: Proceedings of the 34th International Wire and Cable Symposium. 1985. pp. 19-21